Article

Solid-State Nuclear Magnetic Resonance Spectroscopy Studies of Furanose Ring Dynamics in the DNA *Hha*I Binding Site

Gary A. Meints, Paul A. Miller, Kari Pederson, Zahra Shajani, and Gary Drobny

J. Am. Chem. Soc., **2008**, 130 (23), 7305-7314 • DOI: 10.1021/ja075775n • Publication Date (Web): 20 May 2008

JACS
JOURNAL OF THE AMERICAN CHEMICAL SOCIETY

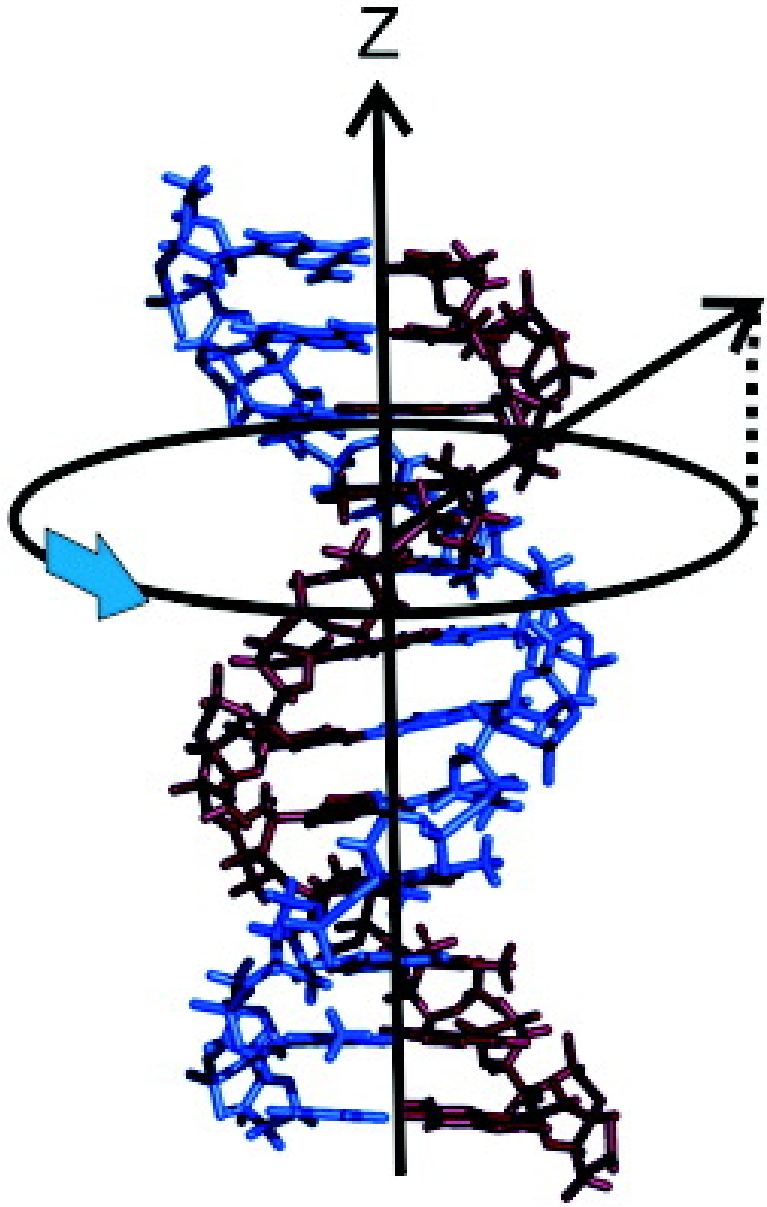

More About This Article

Additional resources and features associated with this article are available within the HTML version:

- Supporting Information
- Links to the 4 articles that cite this article, as of the time of this article download

Journal of the American Chemical Society is published by the American Chemical Society. 1155 Sixteenth Street N.W., Washington, DC 20036

J|A|C|S
ARTICLES

Published on Web 05/20/2008

Solid-State Nuclear Magnetic Resonance Spectroscopy Studies of Furanose Ring Dynamics in the DNA *Hha*I Binding Site

Gary A. Meints,† Paul A. Miller,‡ Kari Pederson,‡ Zahra Shajani,‡ and Gary Drobny*,‡

Department of Chemistry, Missouri State University, Springfield, Missouri 65897, and Department of Chemistry, University of Washington, Seattle, Washington 98195-1700

Received August 1, 2007; E-mail: drobny@chem.washington.edu

Abstract: The dynamics of the furanose rings in the GCGC moiety of the DNA oligomer [d(G_1A_2-$T_3A_4\underline{G}_5\underline{C}_6\underline{G}_7\underline{C}_8T_9A_{10}T_{11}C_{12}$)]$_2$ are studied by using deuterium solid-state NMR (SSNMR). SSNMR spectra obtained from DNAs selectively deuterated on the furanose rings of nucleotides within the 5′-GCGC-3′ moiety indicated that all of these positions are structurally flexible. The furanose ring within the deoxycytidine that is the methylation target displays the largest-amplitude structural changes according to the observed deuterium NMR line shapes, whereas the furanose rings of nucleotides more remote from the methylation site have less-mobile furanose rings (i.e., with puckering amplitudes < 0.3 Å). Previous work has shown that methylation reduces the amplitude of motion in the phosphodiester backbone of the same DNA, and our observations indicate that methylation perturbs backbone dynamics through the furanose ring. These NMR data indicate that the 5′-GCGC-3′ is dynamic, with the largest-amplitude motions occurring nearest the methylation site. The inherent flexibility of this moiety in DNA makes the molecule more amenable to the large-amplitude structural rearrangements that must occur when the DNA binds to the *Hha*I methyltransferase.

Introduction

Methylation of nucleotide bases plays an important role in a host of biological processes,[1–3] from inhibition of cleavage by endonucleases[4] to regulation of transcription-factor binding.[5] In prokaryotic cells, DNA methylation is involved primarily in restriction−modification systems that prevent phage infection. In eukaryotic systems, DNA methylases preferentially act on hemimethylated DNA, where the recognition sequence is simply CG in most animals (hereafter referred to as CpG) and the methylated product is 5-methyl-2′-deoxycytidine.

CpG methylation has important effects on gene transcription in eukaryotes. Many transcription factors, the DNA binding sites of which contain one or more CpG dinucleotides, no longer efficiently bind DNA when their recognition sites are methylated.[6,7] Gene silencing in eukaryotes is thought to result from methylation either directly, by interference with the interaction of the transcription factor with its recognition site, or indirectly, by attracting proteins which have a high affinity for methylated DNA. In addition, abnormal methylation patterns in DNA have been linked to human genetic disorders such as fragile X syndrome.[8] Despite abundant evidence supporting the biological importance of CpG methylation, experimental data do not, as yet, provide a clear picture of the relationship between the functional impact of DNA methylation and the structure of methylated DNA.

The *Hha*I system acts as a defense mechanism in prokaryotic systems to protect the cell from invasive DNA. The system comprises two enzymes, the methyltransferase (Mtase) and endonuclease. Both proteins recognize the sequence [5′-G↓$\underline{C}$GC-3′]$_2$ (the arrow indicates cleavage, and the underlined cytosine base is the methylation target). The Mtase DNA target forms a classic B-form double helix, providing no path to methylate the cytidine base; however, the crystal structure of the *Hha*I Mtase−cognate DNA demonstrates that the cytosine is exohelical and is surrounded in the binding pocket of the Mtase (Figure 1).[9] The physical removal from the stacked base in the helix explains how the methylation position of the base is accessible; however, it is still unknown whether the methyltransferase induces base flipping or captures a conformation where the base is already partly or completely extended out of the helix.

Structural studies of complexes between the *Hha*I Mtase and target DNAs containing a modified and an unmodified CpG step indicate that interactions between the phosphodiester backbone of the DNA and the protein are important components of the recognition process. The crystal structures of the complex *Hha*I and the oligonucleotide with mismatches at the target site in

† Missouri State University.
‡ University of Washington.

(1) Bird, A. *Cancer Surv.* **1996**, *28*, 87–101.
(2) Jones, P. A.; Baylin, S. B. *Nat. Rev. Genet.* **2002**, *3*, 415–428.
(3) Robertson, K. D. *Nat. Rev. Genet.* **2005**, *6*, 597–610.
(4) Ahmad, I.; Rao, D. *Crit. Rev. Biochem. Mol. Biol.* **1996**, *31*, 361–380.
(5) Chela-Flores, J. *Int. J. Theor. Phys.* **1990**, *29*, 853–862.
(6) Adams, R. *Biochem. J.* **1990**, *265*, 309–320.
(7) Adams, R.; Davis, T.; Rinaldi, A.; Eason, R. *Eur. J. Biochem.* **1987**, *165*, 107–115.
(8) Cedar, H. *Cell* **1988**, *53*, 3–4.
(9) Klimasauskas, S.; Kumar, S.; Roberts, R. J.; Cheng, X. *Cell* **1994**, *76*, 357–369.

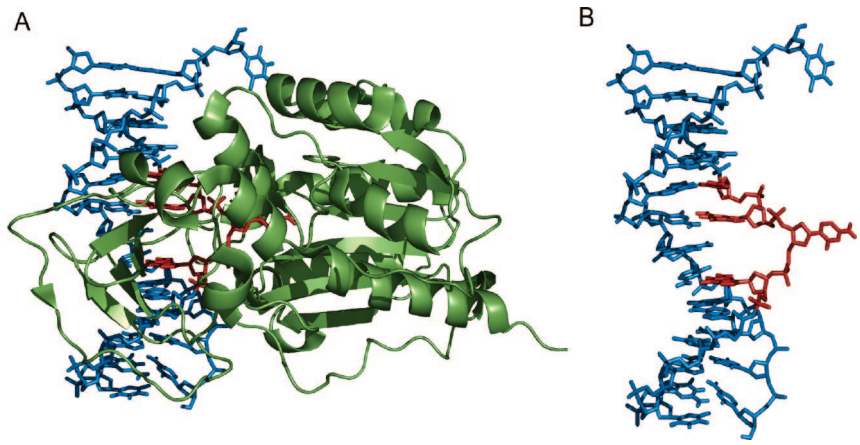

Figure 1. (A) Double-stranded DNA dodecamer [d($G_1A_2T_3A_4\underline{G}_5\underline{C}_6\underline{G}_7\underline{C}_8T_9A_{10}T_{11}C_{12}$)]$_2$ complexed to the *Hha*I methyltransferase. (B) Image of the DNA dodecamer structure in the protein−DNA complex, showing the extrahelical deoxycytidine. The recognition sequence is shown in red.

the DNA, including an abasic site, showed that base flipping still occurs,[10] suggesting that the primary interaction between the protein and the DNA that induces the base-flipping mechanism occurs between the protein and the phosphodiester backbone of the DNA. With such extensive conformational changes of the DNA required for interaction with the Mtase, it is reasonable to expect that some conformational flexibility of the phosphodiester backbone and/or the furanose rings may characterize the native DNA binding site, and that methylation may in turn function as a modulator of this flexibility. However, no quantitative evidence for dynamics of the full 5′-G↓CGC-3′ recognition site has been reported.

Solid-state NMR (SSNMR) has been used to study the internal dynamics of synthetic polymers,[11] liquid crystals,[12,13] nucleic acids,[14–16] and proteins.[17] Deuterium SSNMR is an especially useful probe of molecular dynamics, because the SSNMR line shape and relaxation of deuterium spins are essentially dominated by a single mechanism, the interaction of the nuclear electric quadrupole moment with surrounding electric field gradients. The static quadrupolar interaction varies little from site to site, so relaxation and line shape measurements obtained from chemically distinct deuterons at different sites in macromolecules can be directly compared without the need to correct for variation of the principle elements of the static interaction tensor. In addition, it is not necessary to deconvolute the effects of overall molecular motions and strictly localized internal motions from relaxation data, because overall molecular motions are either quenched entirely in the solid state, shifted to very long time scales, and/or greatly reduced in amplitude.

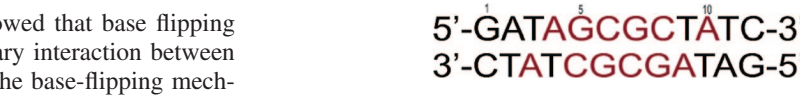

Figure 2. DNA dodecamer containing the target sequence for the *Hha*I protein and DNA dodecamer containing the methylated deoxycytidine. The sites labeled with deuterium and probed in this study are shown in red. The base of C6 is the methylation site.

The combination of deuterium line shape and relaxation data probes a wide dynamic range of motions spanning almost 10 orders of magnitude from nanosecond time-scale dynamics (probed by relaxation measurements), to micro/millisecond time scales (probed by line shape measurements), to even slower motions on the order of seconds that can be probed by monitoring the rate of decay of quadrupolar order.[18]

For this present study, we are interested in using deuterium SSNMR to understand and quantify the extent to which dynamics may assist the protein to recognize methylation sites distributed within the structurally similar B-form DNA double helix and to quantify the degree to which methylation perturbs the local dynamics of the DNA sequence. Previous work suggests that the basis for the specificity of recognition in this system may derive in part from the local dynamics of the DNA, because local flexibility inherent to specific sequences (i.e., GCGC) may lower the barrier for torsion-angle changes, thus making specific sites in a DNA more susceptible to base flipping.

Here, we extend our study of sequence-specific dynamics in CpG-rich DNA oligomers by quantifying furanose-ring dynamics throughout a 5′-G↓CGC-3′ moiety. The conformation of the furanose ring in DNA directly affects phosphodiester torsion angles; therefore, we seek to determine the degree to which phosphodiester backbone mobility in CpG-rich DNAs propagates to the furanose rings. Specifically, we report deuterium SSNMR line shape and relaxation data of the furanose dynamics, both within and adjacent to the 5′-G↓CGC-3′ moiety of the dodecamer [d($G_1A_2T_3A_4G_5C_6G_7C_8T_9A_{10}T_{11}C_{12}$)]$_2$ (Figure 2). In addition, we simulate these line shapes by using a pseudorotation model for the furanose dynamics in order to extract various motional parameters, including amplitudes and both direction and rate of motion. The specific questions that we address here are as follows: how labile is the DNA at and immediately adjacent to the base-flipped nucleotide, and what are the

(10) O'Gara, M.; Horton, J. R.; Roberts, R. J.; Cheng, X. *Nat. Struct. Biol.* **1998**, 5.
(11) Ando, I.; Asakura, T. *Solid State NMR of Polymers*; Elsevier Science: Amsterdan, The Netherlands, 1998.
(12) Emsley, J.; Linfon, J. *NMR Spectroscopy Using Liquid Crystal Solvents*; Pergamon Press: Oxford, U.K., 1975.
(13) Vold, R. Deuterium NMR Studies of Dynamics in Solids and Liquid Crystals. In *Nuclear Magnetic Resonance Probes of Molecular Dynamics*; Tycho, R., Ed.; Kluwer Academic: Dordrecht, The Netherlands, 1994.
(14) Meints, G.; Drobny, G. *Biochemistry* **2001**, *40*, 12436–12443.
(15) Alam, T. A.; Orban, J.; Drobny, G. P. *Biochemistry* **1991**, *30*, 9229–9237.
(16) Wang, A. C.; Kennedy, M. A.; Reid, B. R.; Drobny, G. P. *J. Magn. Reson.* **1994**, *105*, 1–10.
(17) Ravindranathan, K.; Gallicchio, E.; Friesner, R.; McDermott, A.; Levy, R. *J. Am. Chem. Soc.* **2007**, *129*, 474–475.
(18) Spiess, H. *J. Chem. Phys.* **1980**, *72*, 6755–6767.

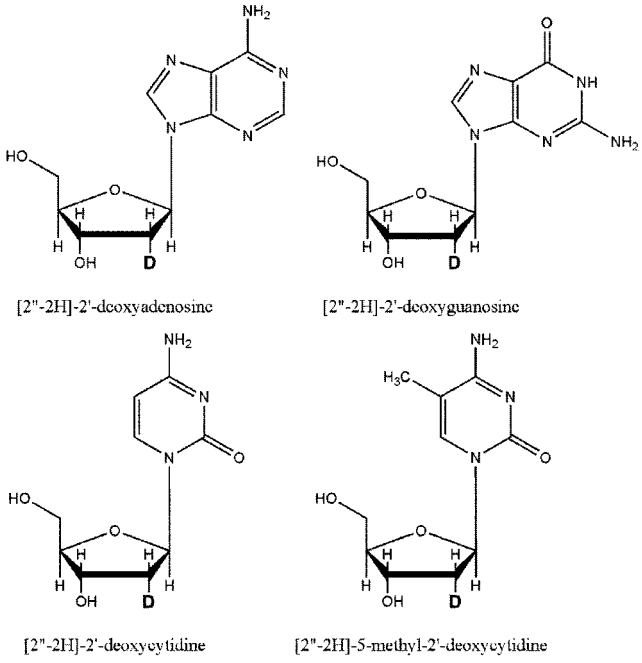

Figure 3. 2′-Deoxyadenosine, 2′-deoxyguanosine, 2′-deoxycytidine, and 5-methyl-2′-deoxycytidine are shown with their deuterium labels.

trajectories of these motions if they are present? In particular, can the amplitudes and rates of local motions at the CpG step be considered characteristic of this particular dinucleotide sequence?

Experimental Section

Chemical Synthesis of Selectively Deuterated DNAs. To investigate furanose-ring dynamics, nucleosides selectively deuterated at the 2′ position of the furanose rings were synthesized (Figure 3) and incorporated into the DNA dodecamer by using phosphoramidite chemistry. Deuteration confirmation is achieved from proton solution NMR of the labeled nucleoside monomers. Loss of signal intensity of the appropriate peaks and changes in splitting patterns of coupled protons are recorded for all labeled monomers. Within the oligonucleotide [d($G_1A_2T_3A_4\underline{G}_5\underline{C}_6\underline{G}_7\underline{C}_8$-$T_9A_{10}T_{11}C_{12}$)]$_2$, deuterium labels were incorporated into the furanose rings of nucleotides A4, G5, C6, G7, C8, and A10. [2″-^{2}H]-2′-deoxycytidine (dC), [2″-^{2}H]-2′-deoxyadenosine (dA), and [2″-^{2}H]-2′-deoxyguanosine (dG) were prepared by the method of Robins et al. with some minor modifications to the solvent systems.[19] Deuterated nucleosides were converted to *N*-acyl-5′-*O*-(dimethoxytrityl)-3′-*O*-(2-cyanoethyl-*N*,*N*-diisopropylphosphoramidite) as described previously.[20]

Deuterated thymidine nucleosides were converted to 5′-*O*-(DMT)-2′-*T*-3′-CED-phosphoramidites as described previously and converted to N4-triazole derivatives.[21] N4-triazole phosphoramidites were incorporated at the 6 position of the growing DNA oligonucleotide sequence by using an ABI model 394 automated DNA/RNA synthesizer. Deprotection of the DNA in concentrated ammonia (2 days, 55 °C) converted the N4-protected thymidine derivative to the 5-methyl-2′-dC nucleotide. The presence of 5-methyl-2′-dC was determined by using both solution NMR and digestion, followed by HPLC analysis (data not shown).

Oligonucleotides were purified on Sephadex size exclusion resin, salted (10% NaCl by weight), packed into a 5 mm SSNMR Kel-F sample chamber, and hydrated by vapor diffusion in a humidity chamber containing saturated salts in ^{2}H-depleted water (75% relative humidity at 20 °C).[22] Water content was quantified gravimetrically by the parameter W (number of water molecules per nucleotide) and is accurate to ±2 water molecules per nucleotide.

SSNMR Spectroscopy. All experiments were performed on a home-built NMR spectrometer, operating at a deuterium Larmor frequency of 76.776 MHz, corresponding to a magnetic field strength of 11.74 T. A quadrupolar echo pulse sequence with an eight-step phase cycling scheme was implemented with a delay of 40 μs between 90° pulses (typically 2.6 μs in duration) and a dwell time of 200 ns during acquisition. Data acquisition was initiated prior to the echo maximum. The time domain data were left-shifted and apodized with 3000 Hz Lorentzian line broadening prior to Fourier transformation. Partially relaxed line shapes and spin-lattice relaxation times were determined by using an inversion recovery pulse sequence, which incorporated a 180° composite pulse to ensure broadband excitation.[23] To obtain powder-averaged Zeeman spin-lattice relaxation times, $\langle T_{1Z}\rangle$, the integrated intensity of the powder spectrum was monitored as a function of the recovery time and analyzed by using a nonlinear least-squares fitting routine.[24]

Theory. The theory of internal molecular dynamics as probed by deuterium SSNMR is well documented,[25] and the following discussion surveys the essential theoretical relationships in order to clarify the approach used to interpret the spectroscopic data. As described in the SSNMR Spectroscopy section, a dynamically modulated deuterium NMR line shape is obtained via a quadrupolar echo experiment. The response of the deuterium spin system starting at the peak of the echo is governed by the equation of motion

$$\frac{\mathrm{d}m(t)_{\pm}}{\mathrm{d}t} = A_{\pm}m(t)_{\pm} \tag{1}$$

where $m(t)$ is the time domain response and

$$A_{\pm} = i\omega_{\pm} + \pi \tag{2}$$

where ± labels either the transition from $m = -1$ to $m = 0$ or from $m = 0$ to $m = +1$ and π is a matrix composed of site exchange rates. $\omega_{\pm}$ is a diagonal matrix with nonzero elements that are the orientation-dependent frequencies

$$\omega_{\pm}^{i} = \pm\frac{3}{4}\frac{e^2qQ}{\hbar}\sum_{a=-2}^{+2} D_{0,a}^{(2)}(\Omega_i^{\mathrm{PC}})D_{a,0}^{(2)}(\Omega^{\mathrm{CL}}) \tag{3}$$

where the super/subscript i denotes the ith of N structural sites. The crystal-fixed frame of the ith site is related to the principal axis system of the electric-field gradient tensor by the solid angle $\Omega_i^{\mathrm{PC}} = (0, \theta_i, \phi_i)$. Because the sample is assumed to be polycrystalline, an additional solid angle $\Omega^{\mathrm{CL}} = (\phi_{\mathrm{CL}}, \theta_{\mathrm{CL}}, 0)$ relates the crystal-fixed frame to the laboratory-fixed frame.

The effect of the second 90° pulse is to reverse quadrupolar precession. Therefore, if detection of the free induction decay is initiated at the top of the echo, the solution of eq 1 is

$$m_{\pm}(t) = \vec{1}\cdot \mathrm{e}^{A_{\pm}(t+\tau_2)}\cdot \mathrm{e}^{A_{\pm}^{*}\tau_1}\cdot \vec{m}_0 \tag{4}$$

where $A_{\pm}^{*} = -i\omega_{\pm} + \pi$. If the matrices T and T^* diagonalize A and A^*, respectively, that is, $T^{-1}AT = \lambda$ and $(T^*)^{-1}A^*T^* = \lambda^*$, the time domain signal may be expanded as

(19) Robins, M.; Wilson, J.; Hansske, F. *J. Am. Chem. Soc.* **1983**, *105*, 4059–4065.
(20) Gait, M. J. *Oligonucleotide Synthesis: A Practical Approach*; Oxford University Press: Oxford, 1984.
(21) Cowart, M.; Gibson, K.; Allen, D.; Benkovic, S. *Biochemistry* **1989**, *28*, 1975–1983.
(22) Weast, R. C., Ed. *CRC Handbook of Chemistry and Physics*, 60th ed.; CRC Press: Boca Raton, FL, 1979.
(23) Tycko, R. *Phys. Rev. Lett.* **1983**, *51*, 775–777.
(24) deFontaine, D.; Ross, D.; Ternai, B. *J. Magn. Reson.* **1975**, *18*, 276–281.
(25) Torchia, S.; Szabo, A. *J. Magn. Reson.* **1982**, *49*, 107–121.

$$m(t) = \vec{1} \cdot T e^{\lambda(t+\tau_2)} T^{-1} \cdot T^* e^{\lambda^* \tau_1} (T^*)^{-1} \cdot \vec{m}_0 = \sum_{j,k,l,m,n} T_{jk} e^{\lambda_k (t+\tau_2)} T^{-1}_{kl} T^*_{lm} e^{\lambda^*_m \tau_1} (T^*)^{-1}_{mn} m_{0,n} = \sum_k b_k e^{\lambda_k t} \quad (5)$$

The orientation-dependent line shape is just the Fourier transform of eq 5

$$I(\omega, \tau_1, \tau_2, \Omega_{CL}) = \mathrm{Re} \int_{-\infty}^{+\infty} m(t) \mathrm{e}^{-i\omega t} \, \mathrm{d}t = \mathrm{Re} \sum_k \frac{b_k}{\lambda_k - i\omega} \quad (6)$$

In a polycrystalline sample, the line shape is averaged over all orientations.

$$I(\omega, \tau_1, \tau_2) = \int_0^{2\pi} d\varphi_{CL} \int_0^{\pi} d\theta_{CL} \sin\theta_{CL} \, I(\omega, \tau_1, \tau_2, \varphi_{CL}, \theta_{CL}) \quad (7)$$

Equation 7 is the theoretical form for the motionally modulated deuterium line shapes presented in this paper. For kinetic models involving jumps between discrete sites, eq 7 is evaluated numerically by using the program MXET1, which also allows calculation of line shapes modulated by motions around multiple axes.[26] In helical DNA, at hydration levels of $W = 10$ and higher, simulations include a uniform rotation around the long helical axis[27] in addition to strictly local motions of the furanose rings and phosphodiester backbone. A second motional axis would require an additional transformation in eq 3, representing the motion around the helical axis.

Spin lattice relaxation rates reported in this paper are obtained from sequences of partially recovered line shapes. Partially recovered line shapes are obtained from a quadrupolar echo pulse sequence that is preceded by a π inversion pulse. Between the π pulse and the first $\pi/2$ pulse of the quadrupolar echo sequence is a period τ_r, during which spin populations relax to their equilibrium values. The partly recovered orientation-dependent line shape is then

$$I(\omega, \tau_1, \tau_2, \tau_\gamma, \Omega_{CL}) = (1 - 2\mathrm{e}^{-\tau_\gamma / T_1}) I(\omega, \tau_1, \tau_2, \Omega_{CL}) \quad (8)$$

In eq 8, the spin-lattice relaxation time for deuterium nuclei is

$$\frac{1}{T_1} = \frac{3}{16} \left(\frac{e^2 q Q}{\hbar} \right)^2 (J_1(\omega, \theta_{CL}, \phi_{CL}) + 4J_2(2\omega, \theta_{CL}, \phi_{CL})) \quad (9)$$

where

$$J_q(q\omega) = \mathrm{Re} \int_{-\infty}^{+\infty} C_q(t) \, \mathrm{e}^{-i\omega t} \mathrm{d}t \quad (10)$$

In eq 10, $C_q(t)$ is the autocorrelation function defined as

$$C_q(t) = \sum_{p,p'} D^{(2)*}_{pq}(\Omega_{CL}) \, D^{(2)}_{p'q}(\Omega_{CL}) \, \langle D^{(2)*}_{0p}(\Omega_{PC}(0)) \, D^{(2)}_{0p'}(\Omega_{PC}(t)) \rangle \quad (11)$$

where

$$\langle D^{(2)*}_{0p}(\Omega_{PC}(0)) \, D^{(2)}_{0p'}(\Omega_{PC}(t)) \rangle = \int \mathrm{d}\Omega_{PC}(0) \int \mathrm{d}\Omega_{PC}(t) \, D^{(2)*}_{0p}(\Omega_{PC}(0)) \, D^{(2)}_{0p'}(\Omega_{PC}(t)) \, P(\Omega_{PC}(t), t | \Omega_{PC}(0)) \, W(\Omega_{PC}(0)) \quad (12)$$

$P(\Omega_{PC}(t), t|\Omega_{PC}(0))$ is the conditional probability of the C−D reorienting to $\Omega_{PC}(t)$, given that it was at $\Omega_{PC}(0)$ at a time t earlier, and $W(\Omega_{PC}(0))$ is the a priori probability of the bond being oriented at $\Omega_{PC}(0)$.

Given eqs 9 and 10, the partially recovered line shape expression in eq 8 also can be numerically evaluated because the spectral densities in eq 9 are orientation-dependent, hence, so is T_1^{-1} (θ_{CL}, φ_{CL}). In this paper, a powder-averaged T_1 refers to the expression

$$\langle T_1^{-1} \rangle = \int_0^{2\pi} \mathrm{d}\varphi_{CL} \int_0^{\pi} \mathrm{d}\theta_{CL} \sin\theta_{CL} \, T_1^{-1}(\theta_{CL}, \phi_{CL}) \quad (13)$$

Models of Furanose Motion. In addition to simulating the motion of the particular sugar ring in question, it is necessary to resolve other types of motion that are present in the sample. For hydration levels as low as $W = 10$, collective-bending and torsional motions are neglected for short DNAs. Also, uniform end-to-end tumbling can be neglected, because this type of motion is restricted in the solid state, even with a sample of intermediate hydration ($10 < W < 20$). Previous work has shown that restricted uniform rotation of the DNA around the helix axis occurs at $W = 10$ and above and is effectively simulated by a six-site jump,[27] with a half angle of $\theta = 20°$ (orientation of the local dynamic axis of the C2′−D bond with respect to the longitudinal helix axis, see Figure 4A), values of $\phi = 0$, 60, 120, 180, 240, and 300° for the six sites, and a rate constant $k \approx 1.0 \times 10^4$ Hz. Use of these parameters for the overall helix motion has produced good agreement in previous work for several different DNA samples with different types of local motions occurring.[27] Here, these parameters are considered well determined and remain constant for the simulations of the local motions. The resulting spectrum is a superposition of the uniform helical rotation and the local motion of the furanose ring.

To simulate the deuterium line shapes for 2″ deuterons in the GCGC moiety, we rely on the fact that the cyclic nature of the furanose ring reduces the number of independent geometrical parameters required to describe the displacement of the C−D bond. The basic structural features of the model used here are due to Herzyk and Rabczenko.[28] In the Herzyk−Rabczenko model, the Cartesian coordinates of the jth heavy atom in the furanose ring are

$$x_j = r_j \left[\sin\alpha_j \times \sin 2\left(\varphi + \frac{4\pi j}{5}\right) - \cos\alpha_j \times \cos 2\left(\varphi + \frac{4\pi j}{5}\right) + R_j \cos\alpha_j \right] y_j = -r_j \left[\cos\alpha_j \times \sin 2\left(\varphi + \frac{4\pi j}{5}\right) - \sin\alpha_j \times \cos 2\left(\varphi + \frac{4\pi j}{5}\right) + R_j \sin\alpha_j \right] z_j = \left(\frac{2}{5}\right)^{1/2} q \cos\left(\varphi + \frac{4\pi j}{5}\right) \quad (14)$$

where, referring to Figure 4B, α_j is the polar angle locating the jth bond, r_j is the radius of the projection of the atomic pseudorotation trajectory onto the plane of the undistorted ring, R_j is the distance from the geometric center of the planar five-membered ring to the center of the projection of the jth trajectory onto the plane of the undistorted furanose ring, q is the puckering amplitude (in Å), and φ is the pseudorotation phase. Given the structural constraints of a furanose ring, the only adjustable parameter is the pucker amplitude q.

Equation 14 describes the coordinates of the heavy-atom framework of the furanose ring as a function of φ. The model can be generalized to include the reorientation of the C−D bond.[29] For each value of pseudorotation phase angle ϕ, there corresponds a set of angles (θ_{PC},φ_{PC}) specifying the orientation of a C−D2″ bond relative to a coordinate system fixed to the framework of the planar furanose ring. The set of angles (θ_{PC},φ_{PC}) is then used to calculate the site frequencies $\omega^i_{\pm}$ according to eq 3. Values for (θ_{PC},φ_{PC}) for the C−D2″ bonds as a function of ϕ and q are given in Table 1.

The trajectory of the 2″ deuteron corresponding to this set of angles is a slightly curved ellipse (Figure 4C). The angular dispersion increases with q. A value of $q = 0.4$ Å is equal to the total excursion along the direction of the major axis of the ellipse of 52°, and the total excursion along the direction of the minor axis is about 20°, whereas for $q = 0.2$, the corresponding excursions along the major and minor semiaxes are about 28° and 10°, respectively.

To calculate the deuterium line shape with eqs 4−6, we need a form for the operator π in eq 2 in addition to trajectory information. Although jumps between discrete sites is a good approximation

(26) Vold R. R.; Vold, R. L. In *Advances in Magnetic and Optical Resonance*; Warren, W., Ed.; Academic Press: San Diego, 1991; Vol. 16, pp 85–171.
(27) Alam, T.; Drobny, G. P. *Chem. Rev.* **1991**, *91*, 1545–1590.
(28) Herzyk, P.; Rabczenko, A. *J. Chem. Soc., Perkin Trans.* **1985**, *2*, 1925–1930.
(29) Meints, G. A.; Karlsson, T.; Drobny, G. P. *J. Am. Chem. Soc.* **2001**, *123*, 10030–10038.

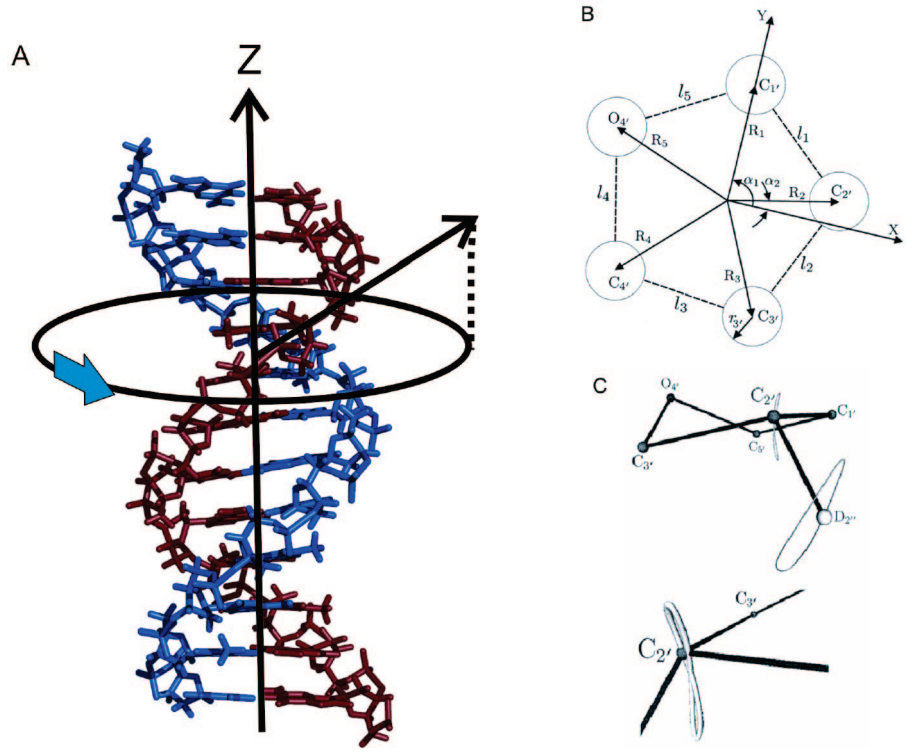

Figure 4. Dynamic axes and coordinate systems used in the studies of furanose ring dynamics. (A) Line shape simulations include two independent motions. A slow (rate of 10^4 Hz) uniform rotation of the DNA molecule occurs about the helical symmetry axis, labeled Z. Local motion of the furanose ring is referenced to a local coordinated system, where the z-axis is indicated by the vector Z_{local}. (B) Coordinate system used to reference local motions of the furanose rings. The coordinate system is defined by the heavy atom framework of the hypothetical planar furanose ring. The circles around each atomic coordinate are the projections of the heavy-atom trajectories onto the plane of the undistorted ring. For example, the trajectory of C3′ is circled around the C3′ coordinate in the planar ring. The radius of this circle is $r_{3'}$. (C) Elliptical trajectories for C2′ and D2″ described by eq 14.

Table 1. Trajectories for the C2′−D2″ Bonds in Terms of the Coordinates θ and ϕ, Referenced to the Coordinate System Shown in Figure 4

	pucker amplitude trajectory (θ, φ)				
pucker phase (deg)	0.2 Å	0.25 Å	0.3 Å	0.35 Å	0.4 Å
0	(79.2, 330.9)	(78.7, 332.3)	(78.2, 333.7)	(77.7, 335.1)	(77.2, 336.6)
36	(81.9, 339.3)	(82.4, 342.3)	(82.8, 345.0)	(83.4, 347.6)	(84.0, 349.8)
72	(85.1, 339.7)	(86.4, 342.6)	(87.8, 345.4)	(89.3, 347.8)	(90.9, 350.1)
108	(86.0, 336.2)	(87.4, 338.8)	(88.8, 341.5)	(90.3, 344.2)	(91.9, 346.8)
144	(84.9, 328.1)	(85.7, 329.0)	(86.6, 330.1)	(87.4, 331.3)	(88.3, 332.7)
180	(83.0, 318.0)	(83.4, 316.1)	(83.8, 314.3)	(84.1, 312.5)	(84.4, 310.8)
216	(81.3, 310.8)	(81.6, 307.0)	(82.1, 303.3)	(82.7, 299.5)	(83.3, 295.1)
252	(79.1, 310.1)	(79.1, 306.2)	(79.3, 302.4)	(79.7, 298.7)	(80.3, 295.1)
288	(76.7, 315.8)	(75.8, 313.3)	(75.0, 310.8)	(74.3, 308.3)	(73.7, 305.8)
324	(76.0, 325.4)	(74.6, 325.6)	(73.1, 325.8)	(71.5, 326.1)	(69.9, 326.4)

when barriers separating the sites approach $10k_BT$, corresponding to a barrier of about 25 kJ/mol at $T = 300$ K, energy computations indicate that much-lower barriers of just a few k_BT separate furanose-ring conformers.[30] Instead of treating the motion of the C−D bond as a jump between discrete sites, the C−D2″ bond can be envisioned as diffusing over these low-energy barriers, and π has the form of a steady-state Fokker−Planck operator

$$\pi = D\left[\frac{\partial^2}{\partial\varphi^2} + \frac{1}{k_BT}U'(\varphi)\frac{\partial}{\partial\varphi} + \frac{1}{k_BT}U''(\varphi)\right] \qquad (15)$$

where $U(\phi)$ is the external potential in which the C−D bond diffuses, and D is the orientation-independent diffusion coefficient associated with the motion of the C−D bond.

Solving eq 1 by using the form for π given in eq 15 is difficult, even for relatively simple forms for $U(\phi)$. Nadler and Schulten[31] have introduced a finite difference approximation for eq 15, where π is represented by a tridiagonal matrix with elements defined by

$$\begin{aligned} &\pi_{ij} = \frac{1}{\tau}\left(\frac{W_i}{W_{i\pm1}}\right)^{1/2}, \quad j = i \pm 1 \\ &\pi_{ij} = -(\pi_{i,j-1} + \pi_{i,j+1}), \quad j = i \\ &\pi_j = 0, \quad \text{otherwise} \end{aligned} \qquad (16)$$

where in eq 16, $W_i = e^{-U(\varphi_i)/k_BT}/Q$, Q is the partition function, and $\tau \approx \delta^2/D$, where δ is the unit of angular displacement that has been used to describe the motion of heme groups in proteins,[32] amino acid side chains in proteins,[33] and lipid chains.[34]

Results

To probe local mobility of the furanose rings in and adjacent to the d($G_5C_6G_7C_8$) site, deuterium line shapes and spin-lattice

(30) Saenger, W. *Principles of Nucleic Acid Structure*; Springer Verlag: New York, 1984.

(31) Nadler, W.; Schulten, K. *J. Chem. Phys.* **1986**, *84*, 4015–4025.

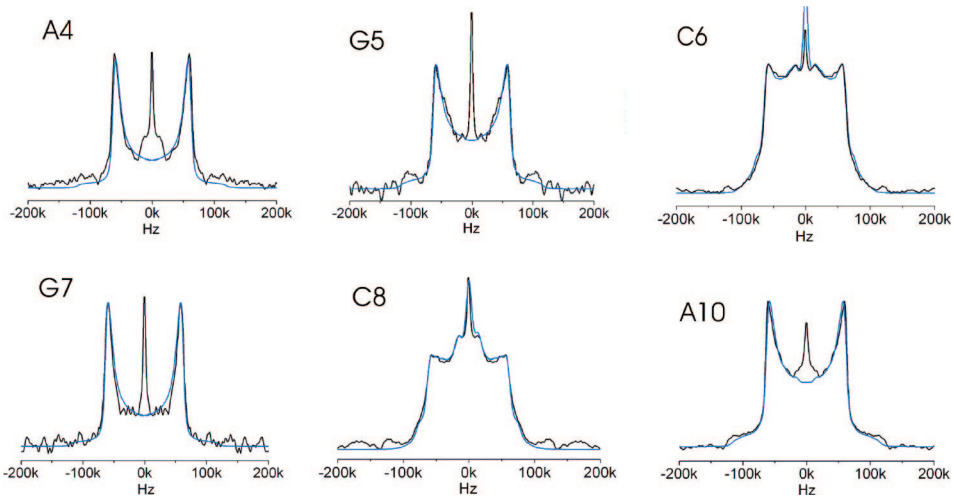

Figure 5. Six deuterium line shapes (black) for each of the labeled sites in the nonmethylated DNA dodecamer with the simulation (blue) of each overlaid. Simulation parameters are described in Table 3.

Table 2. Experimental $\langle T_{1Z} \rangle$ Values for Each of the Seven Labeled Sites

position	hydration (waters/nucleotide)	$\langle T_{1Z} \rangle$ (ms)
[2″-^{2}H]-A4	$W = 12 \pm 2$	65 ± 5
[2″-^{2}H]-G5	$W = 11.0 \pm 1$	59 ± 4
[2″-^{2}H]-C6	$W = 11.5 \pm 1$	29 ± 3
[2″-^{2}H]-G7	$W = 11.3 \pm 1$	69 ± 5
[2″-^{2}H]-C8	$W = 10.4 \pm 1$	22 ± 4
[2″-^{2}H]-A10	$W = 10.2 \pm 2$	82 ± 7
[2″-^{2}H]-5-methyl-C6	$W = 11.0 \pm 1$	25 ± 4

relaxation rates were obtained for the 2″ deuterons of A4, G5, C6, G7, C8, and A10. Experimental line shapes and line-shape simulations are shown in Figure 5. Of the six 2″ deuterium line shapes shown in Figure 5, the line shapes [2″-^{2}H]-C6 and [2″-^{2}H]-C8 are the most strongly perturbed from the Pake doublet form, whereas the furanose rings of A4, G5, and G7 show somewhat weaker deviations from the classic Pake form. Powder-averaged spin-lattice relaxation data for 2″ deuterons in the furanose rings of A4, G5, C6, G7, C8, and A10 are summarized in Table 2.

It is immediately obvious that the $\langle T_{1Z} \rangle$ values for furanose-ring deuterons in the A and G nucleotides within and adjacent to the d(GCGC) segment are distinctly longer than the furanose-ring deuterons of deoxycytidine nucleotides. The $\langle T_{1Z} \rangle$ values for [2″-^{2}H]-A4, [2″-^{2}H]-G5, and [2″-^{2}H]-G7 range from 59 to 69 ms and are comparable within experimental error. The $\langle T_{1Z} \rangle$ value for [2″-^{2}H]-A10 of 82 ms is significantly longer than that for the other purine nucleotides studied. Within the d(GCGC) sequence, the 2″ deuterons in the furanose rings of the C6 and C8 nucleotides have the shortest relaxation times, 29 ± 3 and 22 ± 4 ms, respectively. Clearly, the furanose relaxation and line shape data for A10, which is most remote from the recognition site, show the least indication of dynamic averaging, whereas the furanose relaxation and line shape data for the deoxycytidine nucleotides C6 and C8 within the d(GCGC) moiety show the greatest indication of dynamic averaging.

Analysis of Furanose-Ring Line Shapes. The most common and simple models of furanose-ring dynamics portray it as an exchange between two conformers,[35–38] although recent experimental analyses of proton scalar coupling constants in DNA assume exchange between a greater distribution of conformers.[39] Although activated exchange between discrete conformations of the furanose ring is a good approximation of internal molecular motions when kinetic barriers exceed 25 kJ/mol ($10k_BT$), theoretical estimates of the barrier to exchange between C2′-endo and C3′-endo range from only 2.1 kJ/mol, a remarkably low barrier indicating virtually free pseudorotation, to about 8−21 kJ/mol.[40]

A more realistic model of furanose-ring motion is almost certainly necessary for accurate analysis of NMR relaxation and line shape data. Simulated line shapes in Figure 5 were obtained by setting values for the diffusion coefficient D, the puckering amplitude q, and the potential $U(\phi)$. For [2″-^{2}H]-A4, [2″-^{2}H]-G5, [2″-^{2}H]-G7, and [2″-^{2}H]-A10, best fits are obtained for $U(\phi)$ modeled as a periodic potential of the form

$$U(\varphi) = \frac{U_0}{2}(1 - \cos 2(\varphi - \varphi_0)) \qquad (17)$$

where U_0 is the barrier between the minimum-energy conformers. According to eq 17, the conformational energy displays two wells within the pseudorotation cycle, which occur at $\varphi - \varphi_0 = 0$ and 180°. The motivation for selecting this type of potential for a furanose ring (Figure 6A) shows the effect on the deuterium line shape that results from a variation of D, q, and barrier height U_0 for the potential in eq 17. Table 3 summarizes these parameters for the line shapes that best fit the experimental line shapes for [2″-^{2}H]-A4, [2″-^{2}H]-G5, [2″-^{2}H]-G7, and [2″-^{2}H]-A10. The puckering amplitudes q for these four nucleotide furanose rings range from 0.20 to 0.30 Å, and the barrier heights U_0 range from $4.5k_BT$ to $6k_BT$. Although the simulations specify values for the diffusion coefficients on the order of 10^8 s^{-1} (Table 3), the exchange of the C−D bonds

(32) Nadler, W.; Schulten, L. *Proc. Natl. Acad. Sci. U.S.A.* **1984**, *81*, 5719–5723.
(33) Wittebort, R.; Szabo, A. *J. Chem. Phys.* **1978**, *69*, 1722–1736.
(34) Wittebort, R. J.; Olejniczak, E. T.; Griffin, R. G. *J. Chem. Phys.* **1987**, *86*, 5411–5419.
(35) Altona, C.; Sundaralingam, M. *J. Am. Chem. Soc.* **1972**, *94*, 8205–8212.
(36) Levitt, M.; Warshel, A. *J. Am. Chem. Soc.* **1978**, *100*, 2607–2613.
(37) Bax, A.; Lerner, L. *J. Magn. Reson.* **1988**, *79*, 429–438.
(38) Hatcher, M.; Mattielo, D.; Meints, G.; Orban, J.; Drobny, G. *J. Am. Chem. Soc.* **1998**, *120*, 9850–9862.
(39) Ulyanov, N.; Schmitz, U.; Kuman, A.; James, T. *Biophys. J.* **1995**, *68*, 13–24.
(40) Olson, W. K. *J. Am. Chem. Soc.* **1982**, *104*, 278–286.

Table 3. Model Potentials and Parameters Used To Fit Each of the Line Shapes

label site	$U(\phi)$ (J)	U_0 (J)	κ (J/(mol rad^2))	pucker amp. (Å)	diff. rate (Hz)	r_k (Hz)
A4	$(U_0/2)[1 - \cos(2\phi - 2\phi)]$	$6k_BT$		0.25	4×10^7	1.9×10^5
G5	$(U_0/2)[1 - \cos(2\phi - 2\phi)]$	$4.5k_BT$		0.27	6×10^7	9.5×10^5
C6	$(\kappa/2)(\phi - \phi)^2$		$5k_BT$	0.40	1.8×10^7	
G7	$(U_0/2)[1 - \cos(2\phi - 2\phi)]$	$6k_BT$		0.25	4×10^7	1.9×10^5
C8	$(\kappa/2)(\phi - \phi)^2$		$5k_BT$	0.40	1.8×10^7	
A10	$(U_0/2)[1 - \cos(2\phi - 2\phi)]$	$4.5k_BT$		0.27	2×10^8	3.2×10^6
5mC6	$(\kappa/2)(\phi - \phi)^2$		$5k_BT$	0.35	1.8×10^7	

between the well minima is actually much slower. The escape rates are listed in Table 3.

The rate of exchange between the minima can be estimated from the rate of first passage over the barrier expression by using the expression for the Kramer's escape velocity r_K, truncated to second order[41]

$$r_K \approx \left[-\left.\frac{\partial^2 U}{\partial \phi^2}\right|_{\phi_{min}} \times \left.\frac{\partial^2 U}{\partial \phi^2}\right|_{\phi_{max}} \right]^{1/2} \frac{D}{2\pi k_B T} e^{-U_0/k_B T} \qquad (18)$$

where

$$\left.\frac{\partial^2 U}{\partial \phi^2}\right|_{\phi min}$$

is evaluated at the potential minimum and

$$\left.\frac{\partial^2 U}{\partial \phi^2}\right|_{\phi max}$$

is evaluated at the barrier maximum. For the potential in eq 17,

$$r_K = \frac{D}{\pi}\frac{U_0}{k_B T} e^{-U_0/k_B T} \qquad (19)$$

Very different potential functions were required to fit the line-shape data for [2″-^{2}H]-C6 and [2″-^{2}H]-C8. For these nucleotides, line shapes were best fit by assuming that the C−D bonds reorient over a range of angles without traversing a significant energy barrier. The simplest form for $U(\phi)$ in these cases is a harmonic potential

$$U(\varphi) = \frac{\kappa}{2}(\varphi - \varphi_0)^2 \qquad (20)$$

where ϕ_0 is the point on the pseudorotation path with the minimum energy, assumed here to be 2′-endo, and κ is proportional to the torsional restoring force. As shown in Figure 6B, the line shape is very sensitive to the constants κ and D. The line shapes of [2″-^{2}H]-C6 and [2″-^{2}H]-C8 are best fit by assuming $\kappa = 5\ k_BT$ and $D = 1.8 \times 10^7$ rad^2 s^{-1} (Table 3 and Figure 5). The local dynamics of the furanose rings of [2″-^{2}H]-C6 and [2″-^{2}H]-C8 are virtually the same, the small difference in the centers of the line shapes being due to slightly different levels of HDO in the two samples.

In addition to assuming a different potential function, the puckering amplitudes of the pseudorotational motions of these furanose rings had to be increased to 0.4 in order to simulate the line shapes of [2″-^{2}H]-C6 and [2″-^{2}H]-C8; therefore, these two C−D bonds execute larger amplitude excursions than is the case for the purine nucleotides.

Impact of C6 Methylation on the Furanose-Ring Dynamics. Methylation of the target cytidine base in the 5′-G<u>C</u>GC-3′ moiety perturbs the dynamics of the phosphodiester backbone at C6 in [d(G$_1$A$_2$T$_3$A$_4$<u>G$_5$C$_6$G$_7$C$_8$</u>T$_9$A$_{10}$T$_{11}$C$_{12}$)]$_2$.[14] In the case of the backbone dynamics, we can also frame the discussion by analyzing the quadrupolar coupling constant (QCC):

$$\mathrm{QCC} = \frac{e^2 qQ}{h} \qquad (21)$$

The static QCC for the 5′/5″-methylene deuteron is $\mathrm{QCC}_{static} = 175 \pm 1$ kHz.[15] For deuterium powder patterns that retain a Pake pattern, the amplitude reduction factor (ARF) Λ can be used to assess motional averaging of the QCC. The ARF is defined as

$$\Lambda = \frac{\mathrm{QCC}_{eff}}{\mathrm{QCC}_{static}} = \frac{\left(\frac{e^2 qQ}{h}\right)_{eff}}{\left(\frac{e^2 qQ}{h}\right)_{static}} \qquad (22)$$

and can be roughly equated to an order parameter. For [5′/5″-^{2}H]-C6, the value of 120 ± 2 kHz for QCC_{eff} gives a value of Λ of 0.69. For [5′/5″-^{2}H]-5-methyl-C6, QCC_{eff} is 150 ± 2 kHz, and Λ is 0.86. This numerical indication of spectral broadening implies differential motional averaging in the methylated versus unmethylated DNAs. Motional averaging of the phosphodiester backbone is diminished in the methylated DNA.

If methylation of C6 affects the motion of the phosphodiester backbone, to what extent does it perturb furanose-ring dynamics? The best-fit simulated line shape is obtained for conditions similar to those in the case of the unmethylated DNA, except that the puckering amplitude for the simulation (Figure 7) is $q = 0.35$ Å versus $q = 0.40$ Å in the unmethylated DNA. Therefore, as in the case of the phosphodiester backbone, motional averaging of the furanose-ring line shape for C6 is diminished by methylation.

Discussion

In the present work, we have studied dynamic variations within and near the binding site of the DNA target for the *Hha*I Mtase protein in the DNA sequence in [d(G$_1$A$_2$T$_3$A$_4$-<u>G$_5$C$_6$G$_7$C$_8$</u>T$_9$A$_{10}$T$_{11}$C$_{12}$)]$_2$ by measuring deuterium SSNMR line shape and relaxation data for the furanose rings of A4, G5, C6, G7, C8, A10, and the methylated C6. Deuterium NMR is capable of probing an enormous dynamic range of motion, ranging from less than a nanosecond time scales to millisecond time scales and longer. Motions occurring at rates much greater than the solid-state deuterium spectral width result in pre-averaged line shapes and primarily yield information on the amplitude of motions (i.e., order parameters), whereas motions within the range 10^6-10^9 Hz result in partially averaged line shapes which must be simulated by using a stochastic Liouville equation. In this regime, very detailed information about the trajectories, rates, and energy barriers to structural changes may be obtained.

(41) Risken, H. *The Fokker-Planck Equation: Methods of Solution and Applications*; Springer: Berlin, 1989.

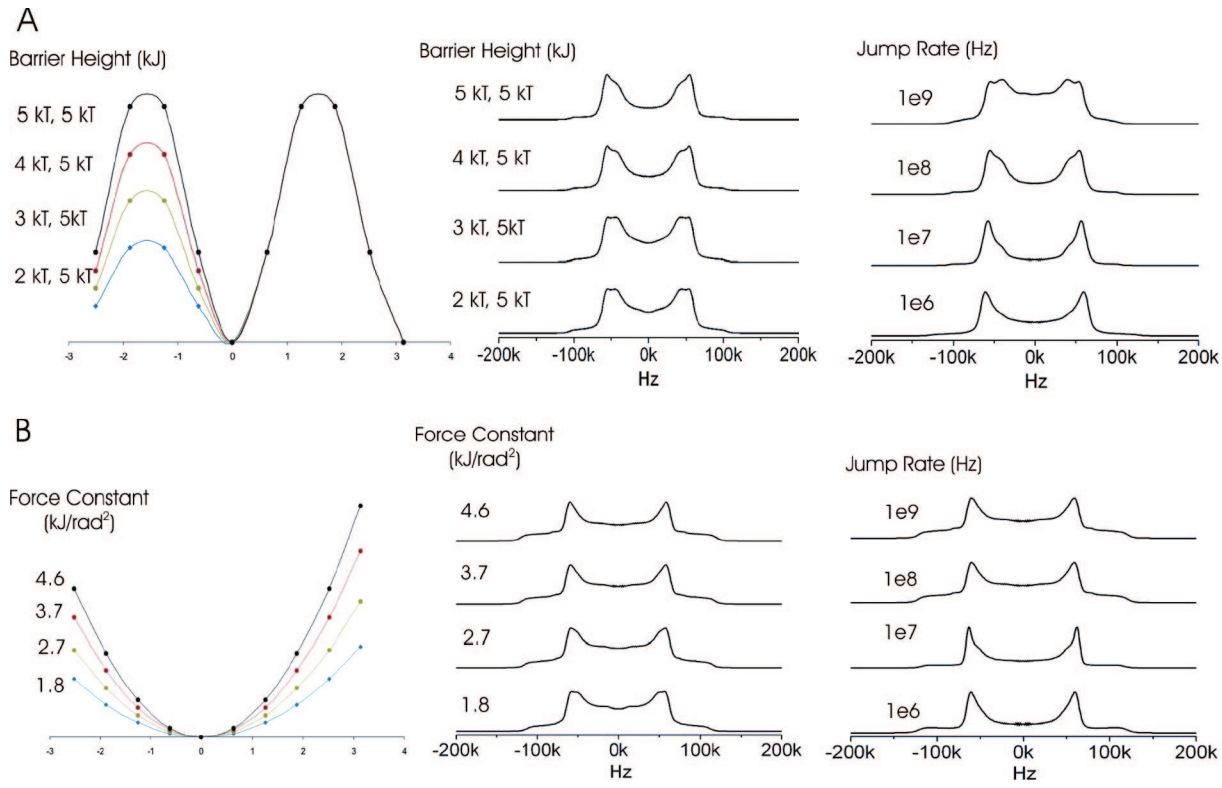

Figure 6. (A) Effect on the deuterium NMR line shape resulting from changing U_0 in the potential equation $U(\phi) = (U_0/2)(1 - \cos 2(\phi - \phi_0))$ and jump rate k. (B) Effect on the deuterium NMR line shape resulting from changing κ in the potential equation $U(\phi) = \kappa/2(\phi - \phi_0)^2$ and jump rate k.

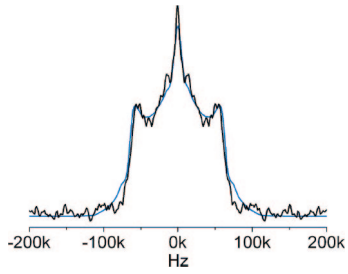

Figure 7. Experimental solid-state deuterium line shape obtained for D2″ in the furanose of methylated C6 (black) and simulated line shape (blue).

The line shapes reported in this study of [d($G_1A_2T_3A_4$-$\underline{G}_5\underline{C}_6\underline{G}_7\underline{C}_8T_9A_{10}T_{11}C_{12}$)]$_2$ indicate that important components of the dynamics of many furanose rings in 5′-G↓CGC-3′ occur in the 10^6-10^9 Hz regime. Although caution must be exerted in the selection of dynamic models for interpreting partially averaged line shapes, furanose rings are so geometrically constrained they require a physically realistic model of furanose motions with few adjustable parameters: the puckering amplitude q, the barrier amplitude U_0 or restoring force constant κ, and the diffusion coefficient D. Line shape and relaxation-rate data indicate that furanose rings in deoxycytidine nucleotides nearest to the methylation site are most dynamic in the sense that they have the largest puckering amplitudes, and the motion of these structures are the least restricted energetically.

Because the furanose rings of both C6 and C8 are mobile to more or less equivalent extents (i.e., have similar puckering amplitudes), the question naturally arises whether the relatively free motion of this structure is characteristic of deoxycytidine nucleotides in this sequence or are all deoxycytidine nucleotides similarly more mobile than the purine nucleotides. Solution ^{13}C relaxation studies of the furanose rings in various DNAs (Shajani and Varani, submitted), including a slightly modified construct of the *Hha*I target DNA, suggest that all the deoxycytidine residues experience more mobility than other residues on the nanosecond to picosecond time scale; however, the recognition site experiences even greater elevated dynamics. Although the number of nucleotides in DNA sequences studied to this thorough extent is limited, a study of deoxycytidine furanose-ring dynamics in a DNA containing a CGCG moiety shows slower motion mobility (nanosecond to microsecond), comparable to that observed for G5 and G7.[29] Therefore, we conclude that the furanose mobilities observed for C6 and C8 are associated with this particular sequence, albeit the database for this kind of information is limited.

Additionally, although the C6 and C8 positions have equivalent simulations, the question arises as to why only the C6 position is methylated. Recognition processes are very complex, and it is not surprising that many factors contribute—among which dynamics may be one. M. *Hha*I makes important protein−DNA contacts with residues within the cognate binding sequence and outside of it.[42] It is possible that the motions within the C8 residue are necessary to form these contacts with this enzyme or with the endonuclease. In particular, the motions might play a role in the interactions with the endonuclease. C8 is an important position within the binding sequence, because it has been shown that cleavage by the *Hha*I endonuclease is completely inhibited by methylation of the C8 position,[43] as well as the target position of the methylase (i.e., C6). Finally, the motions in the furanose ring may not be the only motions that contribute to the protein−DNA interactions. It has been

(42) O'Gara, M.; Horton, J.; Roberts, R.; Cheng, X. *Nat. Struct. Biol.* **1998**, *5*, 872–877.
(43) McClelland, M. *Nucleic Acids Res.* **1981**, *9*, 5859–5866.

shown that there are significant motions in the backbone methylene of the target site (C6)[14] and that this is the only position within the target sequence containing significant motions within the backbone methylene moiety (Pederson et al., accepted).

It is not surprising that the structural flexibility of the DNA backbone near the methylation site is reflected in a similar mobility of the furanose rings, because the structures of the furanose rings and the phosphodiester backbone are not independent. For example, the δ torsion angle, which defines the rotational state of the C3′−C4′ bond, is directly related to the conformation of the furanose ring; therefore, if a given furanose ring is conformationally dynamic, this will be reflected in a change of one or more torsion angles in the phosphodiester backbone. The conformation of the furanose ring also is correlated with other features of the phosphodiester backbone, such as the phosphate−phosphate distance.[30] Therefore, if interactions of a methylating protein with the GCGC recognition site in DNA are made energetically more favorable by a structurally flexible segment of the phosphodiester backbone, this would be reflected by a similar flexibility of furanose rings connected to that region of the backbone. Accordingly, we expect and observe a variation of furanose ring deuterium SSNMR line shapes and relaxation times as we move through the region of the DNA that contains the methylation site.

It is also interesting to note that methylation impacts not only the dynamics of the phosphodiester backbone but the dynamic amplitude of the furanose ring as well. Therefore, methylation may exert its control on the phosphodiester backbone via the furanose ring. The presence of structurally labile furanose rings within the *Hha*I binding sequence resolves the issues of varying degrees of sugar pucker observed in several high-resolution crystal structures. For example, the target-site sugar pucker has been reported to range from C2′-endo−C3′-exo, C3′-endo, to O4′-endo.[44] The presence of the dynamic furanose ring at the target site easily explains the observed variations within these structures. The rmsd of the highest-resolution structure reported is 0.34 Å, and the line shape simulations determine that the repuckering within the mobile sugar rings occurs between approximately 0.2 and 0.4 Å. The dynamics could be easily missed within these structural studies, which appear to observe a snapshot of the dynamic sugar in a particular pucker conformation.

Other techniques have been used to probe the dynamics of DNA, the main one being high-resolution solution NMR. In solution NMR, DNA base, furanose, and backbone dynamics are probed by monitoring the relaxation of the ^{13}C spins.[45–51] Amplitudes and rates associated with motions are extracted from ^{13}C relaxation data by using the model-free formalism of Lipari and Szabo.[52,53] In marked contrast to the solid-state NMR data that we show here, we recently reported that ^{13}C-solution relaxation times across the same DNA sequence are remarkably similar for all residues, with the exception of the terminal A−T pair, where fraying of the base at the end of the helix leads to increased local mobility.[54] Thus, solution-state NMR suggests that internal motions across the *Hha*I methylation target sequence are uniform and unremarkable, as was also reported for the Dickerson dodecamer. In contrast, the solid-state data clearly demonstrate that dynamics across the *Hha*I binding differs along the sequence, particularly at the C6 methylation site.

It is very unlikely that the differences between the two techniques are attributable to different DNA dynamics: DNA motions in the solid state become essentially solution-like, because the DNA becomes hydrated to levels below those used in the present investigation.[16,55] The motions responsible for modulation of the solid-state line shapes likely occur on time scales that are longer than the rate of molecular rotations (3−5 ns for small nucleic acids) and are not easily discernible in solution-NMR relaxation experiments. Other measurements, such as residual dipolar couplings, may be more reliable indicators of molecular dynamics in this regime.[56,57]

Conclusion

The view of sequence-dependent conformational flexibility in DNA and its role in protein recognition and affinity is becoming increasingly important.[58] The most important conclusion from this work arises from the comparison of the dynamics of furanose rings in different nucleotides within the sequence. Local flexibility within the binding sequence could aid the binding by the methyltransferase or the base-flipping process, which is a common motif in numerous protein−DNA interactions. Results from enzymatics,[59] crystallography,[60] and MD[59,60] suggest that furanose-ring flexibility may play a role in M. *Hha*I recognition, as implied by using conformationally constrained sugar derivatives.

For the base-flipping process, there are two competing paradigms on how the mechanism is initiated (active versus passive base flipping). In active flipping, the DNA is in normal B-form when the protein binds. The protein then manipulates the local structure of the DNA, contributing energy to break the necessary hydrogen bonds and altering the local dihedral angles necessary to extrude the target nucleotide. In passive flipping, the enzyme merely senses a transiently flipped base, captures it, and inserts it properly into the binding pocket. There is no definitive conclusion about which method is most likely, because there is supporting evidence for both active[61–63] and passive flipping.[64] Our results support active base flipping, where energetic barriers to the alterations of the local dihedral angles

(44) Shieh, F.; Youngblood, B.; Reich, N. *J. Mol. Biol.* **2006**, *362*, 516–527.
(45) Gaudin, F.; Paquet, F.; Chanteloup, L.; Beau, J. M.; Nguyen, T. T.; Lancelot, G. *J. Biomol. NMR* **1995**, *5*, 49–58.
(46) Boisbouvier, J.; Wu, Z.; Ono, A.; Kainosho, M.; Bax, A. *J. Biomol. NMR* **2003**, *27*, 133–142.
(47) Williamson, J. R.; Boxer, S. G. *Biochemistry* **1989**, *28*, 2819–2831.
(48) Eimer, W.; Williamson, J. R.; Boxer, S. G.; Pecora, R. *Biochemistry* **1990**, *29*, 799–811.
(49) Borer, P. N.; LaPlante, S. R.; Kumar, A.; Zanatta, N.; Martin, A.; Hakkinen, A.; Levy, G. C. *Biochemistry* **1994**, *33*, 2441–2450.
(50) Spielmann, H. P. *Biochemistry* **1998**, *37*, 16863–16876.
(51) Kojima, C.; Ono, A.; Kainosho, M.; James, T. *J. Magn. Reson.* **1998**, *135*, 310–333.
(52) Lipari, G.; Szabo, A. *J. Am. Chem. Soc.* **1982**, *104*, 4546–4559.
(53) Lipari, G.; Szabo, A. *J. Am. Chem. Soc.* **1982**, *104*, 4559–4570.
(54) Miller, P. A.; Shajani, Z.; Meints, G. A.; Caplow, D.; Goobes, G.; Varani, G.; Drobny, G. P. *J. Am. Chem. Soc.* **2006**, *128*, 15970–15971.
(55) Schurr, J. M.; Fujimoto, B. S.; Diaz, R.; Robinson, B. H. *J. Magn. Reson.* **1999**, *140*, 404–431.
(56) Tolman, J. R.; Flanagan, J. M.; Kennedy, M. A.; Prestegard, J. H. *Proc. Natl. Acad. Sci. U.S.A.* **1995**, *92*, 9279–9283.
(57) Tolman, J. R.; Ruan, K. *Chem. Rev.* **2006**, *106*, 1720–1736.
(58) Kalodimos, C.; Boelens, R.; Kaptein, R. *Chem. Rev.* **2004**, *104*, 3567–3586.
(59) Wang, P.; Brank, A.; Banvali, N.; Nicklaus, M.; Marquez, V.; Christman, J.; MacKerell, A. *J. Am. Chem. Soc.* **2000**, *122*, 12422–12343.
(60) Horton, J.; Ratner, G.; Banvali, N.; Huang, N.; Choi, Y.; Maier, M.; Marquez, V.; MacKerell, A.; Chen, X. *Nucleic Acids Res.* **2004**, *32*, 3877–3886.

are significantly lowered in the target site, allowing more easily the conformational changes necessary for proper protein−DNA structural interactions.

Our results suggest that the local dynamics does play an important role in the recognition process, because not only are the dynamics sequence-specific, but the largest motions and lowest energetic barriers occur within the target-site furanose ring itself. From work performed previously, it has been shown that the local dynamics is altered upon base methylation, a result that correlates well with total loss of affinity for the endonuclease and 50-fold reduction in affinity for the methyltransferase. This work supports the conclusion that there is a dynamic aspect of recognition and interaction of the M. *Hha*I enzyme with its recognition sequence.

(61) Huang, N.; Banavali, N. K.; MacKerell, A. D. J. *Proc. Natl. Acad. Sci. U.S.A.* **2003**, *100*, 68–73.
(62) Daujotyte, D.; Serva, S.; Vilkaitis, G.; Merkiene, E.; Venclovas, C.; Klimasauskus, S. *Structure* **2004**, *12*, 1047–1055.
(63) Bellamy, S.; Kruson, K.; Baldwin, G. *Nucleic Acids Res.* **2007**, *35*, 1478–1487.
(64) Cao, C.; Jiang, Y.; Stiver, J.; Song, F. *Nat. Struct. Mol. Biol.* **2004**, *11*, 1230–1236.

Acknowledgment. The authors thank Professors Robert Vold, Gabriele Varani, J. Michael Schurr, and Bruce Robinson for helpful discussions in interpreting relaxation data. This research was supported by a grant from the NIH RO1 EB03152 and a grant from the NSF MCB-0642253.

JA075775N